Materials and Structures (2018) 51:162
https://doi.org/10.1617/s11527-018-1293-x

ORIGINAL ARTICLE

Novel wedge-shaped bond anchorage system for pultruded CFRP plates

Chenggao Li · Guijun Xian

Received: 4 May 2018 / Accepted: 27 November 2018 / Published online: 29 November 2018

Abstract Prestressed strengthening with carbon fiber reinforced polymer (CFRP) plates has gained attention for the rehabilitation of existing structures. In this study, a novel wedge-shaped bond anchorage system was developed. The wedge-shaped adhesive in the bond zones exerted a high pressure on the CFRP plate when the CFRP plate was subjected to tension. The shear force along the fiber direction resisted the tension force of the CFRP plate, realizing reliable anchorage. The shear stress in the anchorage zone was distributed uniformly, owing to the deformation of the low-modulus adhesive. Therefore, the stress concentration was reduced, which generally occurs for traditional CFRP anchors and causes premature failure of the CFRP plate. The stress distribution in the anchorage zone was obtained by mechanical analysis, and the maximum anchorage-bearing capacity was calculated based on the critical bond-slip criterion of the CFRP plate and epoxy adhesive. The effects of the adhesive properties on the anchorage efficiency were also investigated. A test was performed to validate the effectiveness of the proposed anchorage system.

Keywords Anchorage · CFRP plate · Mechanical analysis · Tensile test · Prestressed

C. Li · G. Xian
Key Lab of Structures Dynamic Behavior and Control (Harbin Institute of Technology), Ministry of Education, Harbin 150090, China

C. Li · G. Xian
Key Lab of Smart Prevention and Mitigation of Civil Engineering Disasters of the Ministry of Industry and Information Technology, Harbin Institute of Technology, Harbin 150090, China

C. Li · G. Xian (✉)
School of Civil Engineering, Harbin Institute of Technology, 73 Huanghe Road, Nangang District, Harbin 150090, China
e-mail: gjxian@hit.edu.cn

1 Introduction

During the long-term service lives of concrete structures, flaws, environments, loading and combined factors may lead to the early degradation and deterioration of the components and structures. Rehabilitation, repair or strengthening with appropriate materials are practicable ways to retain the structure in the safe mode [1–5].

In recent years, fiber-reinforced polymer (FRP) composites have been widely used to retrofit reinforced concrete structures owing to their superior features, such as a low weight, high strength-to-weight and stiffness-to-weight ratios, convenient installation, and corrosion and fatigue resistance [6–9]. Carbon fiber-reinforced polymer (CFRP) composites are more advisable and acceptable than glass fiber or aramid fiber-FRPs in some applications owing to their better

mechanical properties and durability [10]. Currently, externally bonded (EB) CFRP plates are well accepted owing to their simple workmanship and convenient construction [10]. However, with this technique, only 20–30% of the tensile strength of the FRPs can be utilized owing to the debonding failure between the CFRP plate and other components (concrete and steel) [11]. The above mentioned problems of the passive EB CFRP systems can be solved using prestressed CFRP plates [12]. In addition to the more efficient strengthening results, there would be more advantages, such as reducing the deflection and crack widths of the strengthened concrete structures, delaying the onset of concrete cracking and yielding of the internal steel reinforcements, removal of the premature debonding failure, and increasing the ultimate load-bearing and shear capacity [11, 13, 14].

The prestressed CFRP strengthening technique requires a near surface mount (NSM), an externally bonded reinforcement (EBR), and external post-tensioning (EPT). For these three techniques, the CFRP anchor method influences the applied prestressing level, major failure modes, and serviceability of the strengthened components [15]. For the NSM without end anchoring, the key failure modes of the strengthened concrete structures are concrete crushing, CFRP debonding, and delamination, while concrete crushing and/or CFRP rupture is achieved if end anchorage is applied [7, 16–18]. In the EBR technique, the failure mode of the strengthened concrete beam with the anchorage is the same as that of the NSM. Triantafillou and Deskovic [19–21] concluded that an additional mechanical anchor at the ends increased the potential of using externally bonded CFRP materials, owing to avoidance of the debonding of FRPs from the concrete substrate and low efficiency of FRPs strengthening. The frequent debonding of the CFRP plate from the strengthened substrate for the EBR without anchorage may lead to an abrupt drop in the load, causing brittle failure [22]. In the EPT technique, end anchorage is applied for the CFRPs, and the desired failure modes of concrete crushing and/or CFRP rupture will occur [23–25]. In addition, Ghafoori et al. [26, 27] developed a prestressed unbounded reinforcement system composed of a pair of mechanical friction clamps to strengthen metallic beams. Trapezoidal, triangular, flat, and contact prestressed un-bonded retrofit systems were considered in the design [28]. Because there is no glue between the CFRP plates and the beams, the surface preparation time and cost of retrofitting was reduced. Furthermore, the clamps were the most important elements of the system for the design consideration. In conclusion, anchorage of the CFRP plates for structural strengthening would ensure the long-term safety of strengthened concrete structures.

Currently, numerous anchorage systems have been reported for CFRP plates. The main types include metallic and nonmetallic anchors. Metallic anchors are divided into a mechanical anchor [29, 30], adhesive bonding anchor [31], and hybrid anchor [32], according to the stress transfer in the anchorage zone [33–35]. Because of the strengthened CFRP plate's large width-to-thickness ratio, it is a potential advantage to apply the adhesive to transmit the load to the metal connectors. For the adhesive, a satisfactory bonding strength with the CFRP plate and ductility are the two important design parameters to ensure anchorage efficiency and long-term service reliability under cyclic dynamic loads. A ductile adhesive is applicable for the bonding medium, and it can dissipate the strain energy of the CFRP plates and avoid stress concentration of the CFRP plates. A rectangular steel plate could be chosen as the metal connector, and the bolts could connect the steel plates to the strengthened components, such as a steel beam, concrete beam, and slab.

Wu et al. [32] proposed a hybrid anchorage system (Fig. 1), including adhesive bonding and mechanical fastening. The mechanical fastening anchorage was formed by fixing two anchor plates with screws and connecting the concrete beam with plate lugs using a welding technique. The bonding anchorage was achieved by the chemical anchor bolts and adhesive bonding between the two anchor plates. The adhesive bonding of the FRP and anchor plates was enhanced by the mechanical anchorage and friction that

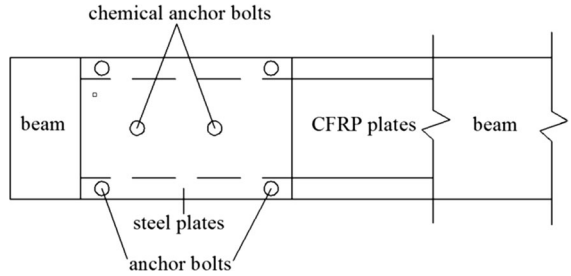

Fig. 1 Schematic diagram of anchorage system of loaded-end anchorage (Wu et al. [32])

developed. Two problems in the hybrid anchoring system were found. The welded connection could lose its long-term function under dynamic loads and steel corrosion. In addition, the chemical anchor bolts were placed in a hole drilled through the CFRP plate, which could cause damage. El-Hacha et al. [36] adopted a mechanical steel plate anchor to prestress the CFRP sheet and plate (Fig. 2). In this method, the CFRP sheet or plate was bonded and extruded between the steel plate anchor and strengthened components. The steel plate anchor was also fixed to the strengthened components by a bolt. The interfaces of the steel anchorage/CFRP/strengthened components had potential bonding failure owing to direct exposure to the service environment, leading to stress loss of the CFRP and degradation of the load-bearing capacity of the strengthened component. Furthermore, local damage could occur on the CFRP plate surface close to the anchorage end during the gripping and extrusion because of the stress concentration. Kim et al. [37] developed a U-wrap nonmetallic anchor system using a transverse CFRP sheet to replace the metallic anchor to strengthen the concrete beam with the prestressed CFRP sheet. The authors indicated that maintaining the initially transferred prestress in the longitudinal CFRP sheets was a critical concern and should be solved in the future after removing the steel anchors.

Therefore, a simple and durable anchorage system is imperative to solve the problems of existing metallic and nonmetallic anchors. The new design is required to avoid damage of the CFRP plates during prestressing and realize a reasonable and reliable stress transferring between the steel anchor and CFRP plate. In addition, the long-term durability of the anchorage system should satisfy the service requirements in extreme environments. Easy preparation and a low cost are also required for practical application. In this study, a novel wedge-shaped bond anchor was proposed. The anchoring mechanisms were analyzed based on numerical and mechanical methods. Experimental tests were also performed to validate the design, and the effects of the applied adhesives were investigated.

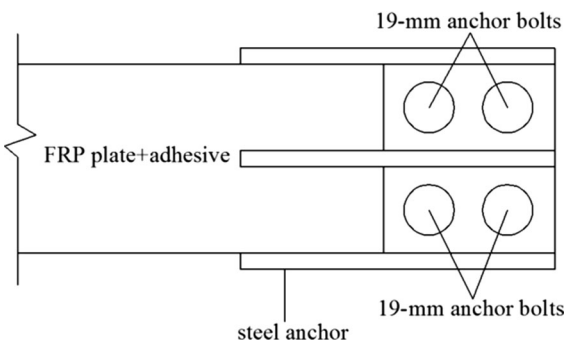

Fig. 2 Fixed anchor installed at the end of the beam (El-Hacha et al. [36])

2 Experimental program

2.1 Raw materials

The CFRP plates were manufactured by a pultrusion technique using methyl tetrahydrophthalic anhydride as a propriety epoxy formulation. The dimensions of the CFRP plate were 25 mm × 1.5 mm, and the fiber volume content was approximately 60%. The average tensile strength, elastic modulus, and elongation of five samples using an aluminum plate anchor were 1.95 GPa (± 0.12), 168.4 GPa (± 1.4), and 1.16% (± 0.08), respectively.

Two epoxy adhesives, T1 and Tc (Shandong Dagong Company, Linyi, China), were used for the wedge shaped adhesives for anchorage. Tc is a tough adhesive with low modulus, low strength and high strain at failure; T1 is a linear elastic adhesive. The properties of T1 and Tc are given in Table 1.

2.2 Wedge-shaped bond anchorage system

Inspired by the clamping and tensioning mechanisms of a universal testing machine, wedge grooves with a width, depth, and gradient could be processed inside the steel plate to simulate the loading process of the tensile clamp. By filling the adhesive into the wedge grooves, the formed wedge adhesive element transferred the stress between the CFRP plate and steel plate through chemical bonding and physical extrusion. A mold release agent was applied on the surface of the steel wedge groove to allow the wedge epoxy element to be easily extruded from the steel wedge groove and generate the pressure force on the CFRP plate. The pressure increased with the extruded wedge-shaped epoxy elements, and the enhanced pressure force led to a high frictional force in the adverse direction to the tension of the plate. Together with the chemical bonding of the adhesives, the

Table 1 Mechanical properties of two filled adhesives

Adhesive type	Tensile properties			In-plane shear strength (MPa)	Interface bond strength with CFRP plate (MPa)[a]
	Tensile strength (MPa)	Tensile modulus (GPa)	Ultimate elongation (%)		
T1	53.60 (± 1.90)	3.51 (± 0.11)	3.01 (± 1.53)	33.49 (± 0.53)	19.01 (± 0.38)
Tc	25.60 (± 0.34)	1.43 (± 0.07)	10.65 (± 0.11)	22.25 (± 0.38)	30.63 (± 2.59)

[a]The interface bond strength was obtained through anchoring CFRP plate in the wedge-extrusion bond anchor. The total anchoring length of CFRP plate was 60 mm, including 40 mm' net bonding length and 20 mm' position fixing length. Two samples were tested to obtain the average

frictional force was designed to anchor the CFRP plates.

The wedge-shaped bond anchor is schematically shown in Fig. 3 for the specific CFRP plate. The total length of the anchor was 240 mm, including four wedge grooves of 160 mm to bond with the CFRP plate and two plat grooves of 80 mm at both ends of the anchor to fix the position of the CFRP plates. For the wedge grooves, each length along the CFRP plate was 40 mm. The maximum depth was 10 mm, and the widths were 60 mm, 50 mm, 40 mm, and 30 mm. The different groove widths were designed to determine the most unfavorable section and to conduct a conservative mechanical analysis. Based on the thickness of the CFRP plate (1.5 mm), the flat grooves at both ends were 40 mm × 27 mm × 1.5 mm for the fixed anchor end and 40 mm × 27 mm × 3 mm for the tension anchor end. The larger flat groove thickness (3 mm) on the tension end was to avoid stress concentration between the CFRP plate and steel plate surface owing to the direct friction contact.

Based on the width of the CFRP plate (25 mm), the maximum diameter of the bolt (20 mm), and the specified minimum space among the bolt, steel plate outer edges, and wedge groove inner edges, the width of the steel plate was determined to be 120 mm from an economic perspective. Finally, the size of the two anchor steel plates was 240 mm × 120 mm × 30 mm.

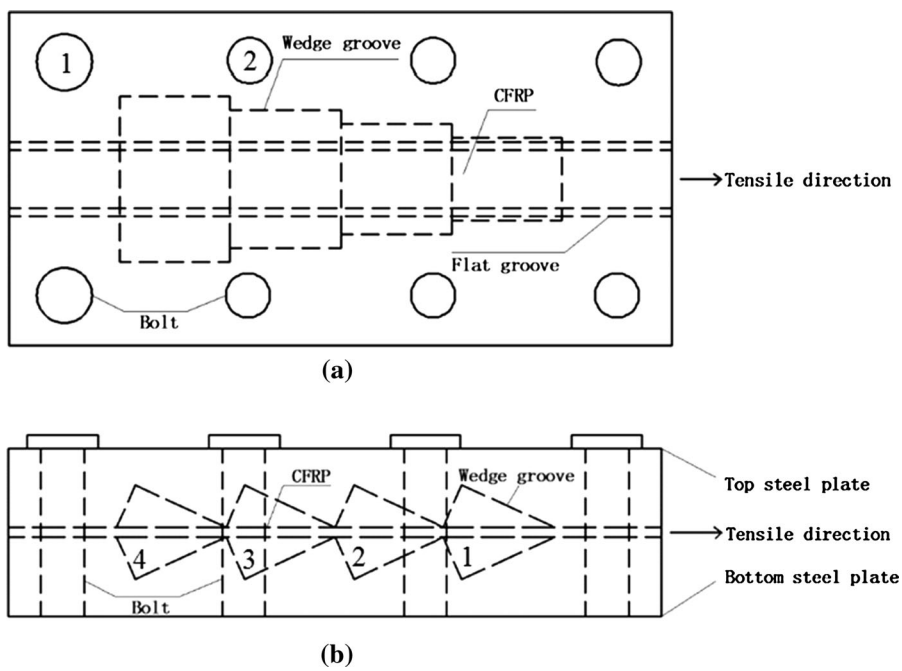

Fig. 3 Design sketch of anchorage system of **a** planar graph; **b** back elevation

2.3 Validation test of the anchor

Before the tensile test of the CFRP plate, two anchoring methods were adopted by the wedge-shaped bond anchor. In addition, the aluminum plate anchor was applied to both ends of the CFRP plates to obtain the control tensile strength of the CFRP plate. The first and second anchoring methods were mixed-type anchors, including the aluminum plate anchor at one end and the developed wedge-extrusion bond anchor at the other end. Two adhesives (Tc and T1) were chosen as the fillers. The third anchoring method employed the wedge-extrusion bond anchor at both ends of the CFRP plates to simulate the prestressed tensioning process of the CFRP plates, and the filler was the Tc adhesive. Specifically, the anchoring process of the CFRP plate with the wedge-extrusion bond anchor included the following steps. First, the CFRP plate was polished in the bond region along a $\pm$ 45° angle, and the impurities remaining in the CFRP plates were removed with acetone solvent. Then, a brush was used to remove the residual scrap iron in the steel wedge groove, and the mold release agent was evenly applied on the steel wedge groove surface of the two anchors. Subsequently, the CFRP plate was placed in the flat grooves at both ends of one anchor and aligned with the center line of the plate grooves. Another anchor was fixed on the above anchor with high-strength bolts. To avoid outflow of the filled epoxy, the gaps of the two anchors up and down were sealed with adhesive tape. In addition, the flat groove in the tension end was levelled with a plastic pad to ensure the central position of the CFRP plate in the anchor. After the above preparations were completed, the filled adhesive was injected into the wedge grooves using a high-pressure injector. The epoxy overflowing from the holes was removed with the acetone solvent. Finally, the filled adhesive of the anchor system was cured for 24 h at room temperature and was transferred to an oven to cure for 24 h at 60 °C based on T_g of the filled epoxies.

After the preparation of the anchorage system, the validation tests of the anchor were conducted according to ASTM D 3039 using a universal tensile machine (DHY-10080, Shanghai, China), as shown in Fig. 4. The crosshead displacement rate was set to 5 mm/min. Two samples were prepared, and the average results were reported.

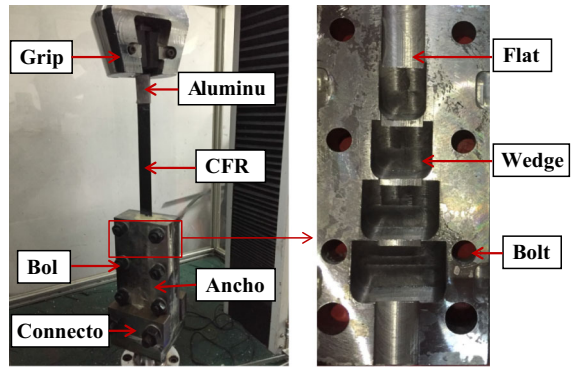

Fig. 4 Tensile test of anchorage system

3 Results and discussion

3.1 Mechanical analysis of the wedge-shaped bond anchorage

As shown in Fig. 3, the anchor included four wedge-shaped groove elements with the same anchorage length l, and the gradient angle of each wedge element was Φ. Anchorage was realized through chemical bonding and friction along the CFRP plate owing to the pressure from the steel plate to the wedge-shaped adhesive. Its mechanical model is shown in Fig. 5. In the model, the ultimate tensile strength and nominal size of the CFRP plate were σ_c and $b \times t$, respectively. After analyzing the four wedge-shaped grooves, the element number in the anchor was extended to n for a general situation.

Before the mechanical analysis, some assumptions were made for simplifying the calculation. The four wedge groove elements sustained the tensile load through the chemical bonding and physical extrusion of the CFRP plate, wedge epoxy, and steel plate. Specifically, the external load (F_0) was balanced with the maximum interface bond-friction (F_f) of the CFRP/adhesive. Furthermore, the interface bond-friction (F_f) was considered a complex combination, including the static friction and cohesive force between the CFRP plate and wedge adhesive, and the interface bond-friction coefficient was μ. The flat groove at both ends of the anchor had no contribution on the bearing capacity of the anchor. The interface shear force and reacting forces were assumed to be the same in the four epoxy elements.

Figure 5 shows the force analysis when the CFRP plate was subjected to tension, F_0. As shown, four

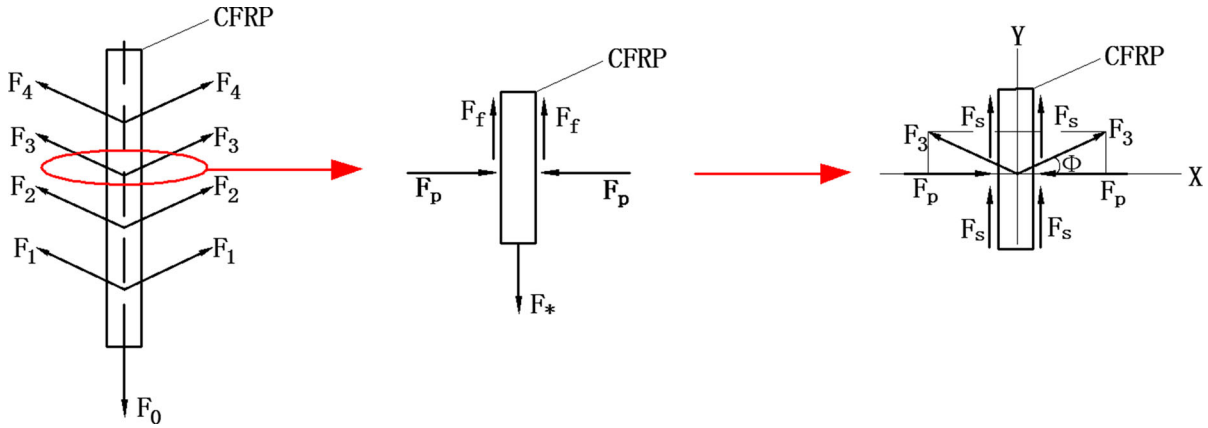

Fig. 5 Mechanical model diagram of anchorage system

reacting pressure forces, F_1, F_2, F_3, and F_4, were provided by the wedge-shaped adhesive and acted on the CFRP plate to balance F_0. For each wedge-shaped adhesive element, the reacting force F_1–F_4 could be decomposed orthogonally into two forces, the normal pressure F_p and shear force F_s along the x- and y-coordinates. The normal pressure F_p, increased the static frictional force, F_f. The shear force F_s caused debonding destruction of the CFRP/adhesive when the average interface shear stress ($\sigma_{s,ave} = F_s/A_s$, where A_s is the shear area) exceeded the bond strength σ_b of the CFRP/adhesive. For $\sigma_{s,ave} > \sigma_b$, interface debonding failure occurred. For $\sigma_{s,ave} = \sigma_b$, the critical condition was obtained, and when $\sigma_{s,ave} < \sigma_b$, fracture of the CFRP plate occurred, and the anchor provided more than 100% anchorage bearing capacity. Here, σ_b was related to the CFRP plate surface properties, epoxy properties, and anchorage length. The parameter $\sigma_{s,ave}$ was dependent on the shear stress distribution and bond-friction coefficient, as discussed below.

When assuming the ultimate tensile strength and nominal size of the CFRP plate was σ_c and $b \times t$, respectively, the ultimate tensile load of the CFRP anchorage system was $F_0 = \sigma_c \times b \times t$. Taking element 3 as an example, the load applied on each element was F^* and its value was equal to $F_0/4$. According to the mechanical equilibrium condition, the maximum interface bond-friction F_f for each element was obtained.

$$F_f = \frac{F_*}{2} \tag{1}$$

According to the bond-friction coefficient μ, the normal pressure F_p was determined.

$$F_p = \frac{F_f}{\mu} \tag{2}$$

Furthermore, the reacting forces F_3 from wedge adhesive element 3 were calculated using the cosine value of gradient angle Φ.

$$F_3 = \frac{F_p}{\cos\phi} \tag{3}$$

Meanwhile, the interface shear force F_s of the CFRP/adhesive was determined as follows.

$$F_s = F_p \times \tan\phi \tag{4}$$

For element 3, the shear area A_s was the interface contact area of the CFRP/adhesive and was obtained as $A_s = b \times l$. Finally, the average shear stress $\sigma_{s,ave}$ in element 3 and the other elements was deduced.

$$\sigma_{s,ave} = F_s/A_s = \frac{\sigma_c t}{8\mu l}\tan\phi \tag{5}$$

For the anchor with n elements, the average shear stress $\sigma_{s,ave}$ in each element was as follows.

$$\sigma_{s,ave} = \frac{\sigma_c t}{2n\mu l}\tan\phi \tag{6}$$

The parameters σ_c and t were the ultimate tensile strength and thickness of the CFRP plate. The parameter n was the wedge element number, and μ was the interface bond-friction coefficient. The parameter l was the bond length of each element, and Φ was the gradient angle of each wedge element.

From Eq. (6), the average shear stress was mainly dependent on the total anchorage length, interface bond-friction coefficient, and element gradient angle. The anchorage length and element gradient angle were two important design parameters, and the interface bond-friction coefficient was determined by the interface bond and friction properties of the CFRP/adhesive. In this study, the ultimate tensile strength and nominal size of the CFRP plate was considered to be 2100 MPa and 25 mm × 1.5 mm, $n = 4$, $l = 40$ mm, $\tan \Phi = 0.4515$, and $\mu = 0.4$, respectively, when referred to the friction coefficient between GFRP plate and steel plate ($\mu = 0.5$). The nominal thickness of the CFRP plate was based on the general size of the CFRP plate in strengthening applications. The nominal strength of the CFRP plate considered the minimum tensile strength of the CFRP plate in the strengthening applications. The aim of thickness and strength modification was to increase the applicability of the bearing capacity checking of anchor. Substituting these parameters into Eq. (6), the average shear stress $\sigma_{s,ave}$ in each element was 11.12 MPa.

Furthermore, the critical failure condition of the anchor was expressed as follows.

$$\sigma_b = \frac{\sigma_c t}{2n\mu l} \tan \phi \tag{7}$$

The parameter σ_b was the interface bond strength of the CFRP/adhesive for each wedge element, and it was relevant to the mechanical properties of the adhesive and the surface property of the CFRP plate. When considering the interface failure condition of the adhesive, σ_b was amended as the maximum of the interface bond strength of the CFRP/adhesive, tensile strength, and shear strength of the adhesive and was expressed as follows.

$$\sigma_b = \max(\sigma_{C/a},\ \sigma_t \text{ and } \sigma_s) \tag{8}$$

The parameter $\sigma_{C/a}$ was the interface bond strength of the CFRP/adhesive, and σ_t and σ_s were the tensile and shear strength of the adhesive, respectively. Finally, the critical failure condition of the anchor was determined as follows.

$$\max(\sigma_{C/a},\ \sigma_t \text{ and } \sigma_s) = \frac{\sigma_c t}{2n\mu l} \tan \phi \tag{9}$$

As shown, the critical failure condition required the interface bond strength of the CFRP/adhesive and the tensile and shear strength of the adhesive. To study the effect of the adhesive on the anchoring efficiency, two structural epoxy adhesives, T1 and Tc, were applied, and their mechanical properties and interface bond strength with the CFRP plate are listed in Table 1. As shown, the T1 epoxy had a higher tensile, higher shear properties and lower deformation capacity. Conversely, the interface bond strength of the CFRP plate was lower and became the anchorage-controlling factor. For the Tc adhesive, a higher interface bond strength was achieved, and its tensile strength was surpassed. The low shear strength turned into the weakest point of the anchor. When the tensile properties of the CFRP plate were high, the anchoring failure mode of the anchor with the T1 adhesive was predicted to be debonding of the CFRP plate from the adhesive, and the failure mode of the anchor with the Tc epoxy was the shear failure of the adhesive. Thus, the adhesive had a significant influence on the anchoring failure mode owing to the different mechanical properties.

After comparing the mechanical parameters of the two adhesives (Table 1), the minimum interface bond strength $\sigma_{b,T1\text{-}60\ mm}$ (19.01 MPa) of the CFRP/T1 adhesive was chosen as the critical failure condition of the anchor. From the critical condition, the failure mode of the anchors with Tc and T1 adhesives was fracture failure of the CFRP plate, and there was no interface debonding of the CFRP/adhesive.

For the critical failure condition [Eq. (9)], there were two uncertainties to be determined. One was the distribution of the interface shear stress along the anchoring length, and the other was the evaluation of the bond-friction coefficient μ. Therefore, some discussions and analysis were performed to obtain the critical interface shear stress. Figure 6 shows the interface shear stress distribution of each element for three different bond-friction coefficients, 0.4, 0.5, and 0.6, and two possible shear stress distribution trends, linear and nonlinear (quadratic) distributions. Here, the quadratic distribution of the interface shear stress of the CFRP/adhesive simulated the nonlinear trend. The interface shear stresses in elements 1 and 4 were considered to be the maximum and minimum, respectively, and the relationship of them was assumed to be $\sigma_{s,max} = 3\sigma_{s,min}$ for the linear and nonlinear distributions. The estimation of the relationship ($\sigma_{s,max} = 3\sigma_{s,min}$) was determined from the He et al. experiment [38].

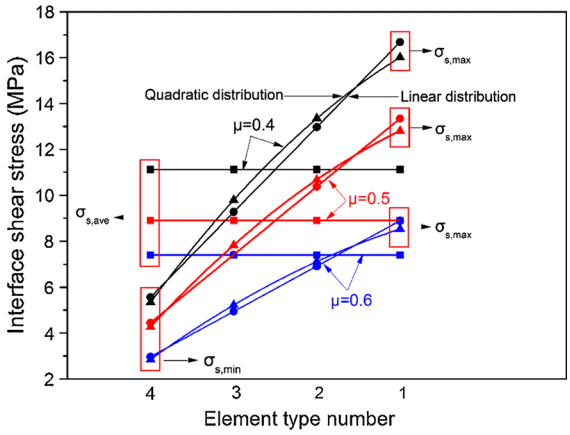

Fig. 6 Interfacial shear stress analysis in each element

As shown, the interface bond-friction coefficient μ had a significant influence on the interface shear stress distribution of the CFRP/adhesive. The average interface shear stress $\sigma_{s,ave}$ was proportional to the bond-friction coefficient μ, and the values were 7.41 MPa, 8.90 MPa, and 11.12 MPa for μ = 0.6, 0.5, and 0.4, respectively. There was minimal impact of the linear and nonlinear distributions on the interface shear stress. The maximum interface shear stress appeared in element 1 and was referred to as $\sigma_{1s,max\text{-}0.4\ L}$ for the linear distribution, when the bond-friction coefficient was μ = 0.4. Its value was 16.68 MPa, nearly two times that of μ = 0.6, $\sigma_{s,max\text{-}0.6\ L}$ = 8.90 MPa. Based on the failure criterion, $\sigma_{1s,max\text{-}0.4\ L}$ = 16.68 MPa < $\sigma_{b,T1\text{-}60\ mm}$ = 19.01 MPa, the CFRP/adhesive interface did not reach failure when the CFRP plate reached its material limit state. In addition, the interface bond-friction coefficient μ = 0.4 was conservative when referred to the friction coefficient (μ = 0.5) of the GFRP plate/steel plate because the interface of the CFRP/adhesive combined physical extrusion and chemical bonding to form a complex and powerful interface. From the theoretical analysis, the bond-friction coefficient μ was larger and could be more than 0.6. When μ = 0.6, the interface shear stress $\sigma_{s,max\text{-}0.6\ L}$ was 11.12 MPa, less than the bond strength of $\sigma_{b,T1\text{-}60\ mm}$ (19.01 MPa).

For the wedge-extrusion bond anchor, the extrusion force between the wedge steel plate and epoxy played a significant role on bearing the external load. After evaluating the interface bearing capacity of the CFRP/adhesive, the compressive bearing capacity of the wedge steel grooves should be determined when the extrusion reaction force from the wedge epoxy acted on the wedge steel plate. Specifically, when the external load F_0 was applied to the CFRP plate, the extrusion force (F_1, F_2, F_3, and F_4) between the steel plate and epoxy formed through the CFRP/adhesive interface bonding transfer and the extrusion force on the wedge steel plate, marked as F_{e1}, F_{e2}, F_{e3}, and F_{e4}. Figure 7 shows the mechanical analysis model of the wedge steel plate of element 1. Here, element 1 was chosen as the most unfavorable element to evaluate the compressive bearing capacity, because the compressive area A_e of element 1 was smaller; however, the extrusion force F_{e1} was larger. Based on the above analysis, the most unfavorable condition was when the interface bond-friction coefficient was μ = 0.4, and the shear stress presented a linear distribution.

The maximum shearing force of element 1 was obtained from the maximum interface shear stress $\sigma_{1s,max\text{-}0.4\ L}$.

$$F_{s1,max} = \sigma_{1s,max-0.4L} \times A_s \tag{10}$$

From the relationship between the shear force and extrusion force, the extrusion force F_1 was obtained.

$$F_1 = F_{s1,max} / \sin\phi \tag{11}$$

By using the law of action force and reaction force, the reaction force F_{e1} on the steel plate was equal to F_1. Finally, the maximum pressure stress Q on the steel plate was determined.

$$Q = F_{e1}/A_e = \frac{\sigma_{1s,max-0.4L} \times b \times l}{\sin\phi \times A_e} \tag{12}$$

The parameter $\sigma_{1s,max\text{-}0.4\ L}$ was the maximum element shearing stress after considering the most unfavorable conditions, and A_e was the extrusion area of the wedge steel plate. Substituting these parameters

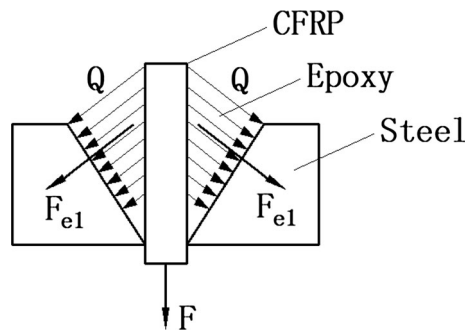

Fig. 7 Mechanical analysis of wedge steel plate

into Eq. (12), the maximum pressure stress Q on the steel plate was 69.48 MPa, which was less than its ultimate compressive strength (235 MPa). The steel plate was in an elastic working state.

To validate the anchorage bearing capacity of the anchor, a tensile test of the anchor was conducted by connecting the bolt of the anchor to the tensile machine base. As shown in Fig. 3, there were two types of bolts with different diameters, referred to as bolt 1 and bolt 2. The diameter of bolt 1 was 20 mm, and its function was to fix the anchor to the tensile machine base. The diameter of bolt 2 was 16 mm, and its function was to fix the two steel plates of the anchor. Before the tensile test of the anchor was conducted, the shear-bearing capacity of bolt 1 was evaluated. In addition, the section of two steel plates was weakened and the tensile bearing capacity should be determined.

The calculation included the shear-bearing capacity of the bolt and the tensile bearing capacity of the steel plate. The shear-bearing capacity N_{vb} of a single bolt was obtained based on the equation below.

$$N_{vb} = 0.9 \times n_f \times \mu \times P \tag{13}$$

Here, 0.9 was the inverse of the resistance factor γ_R, and n_f was the number of the transmission friction surface. The parameter μ was the anti-sliding coefficient, and P was the design values of the pretension force of the bolt (Φ 20).

From the reference standard of the steel structure, $n_f = 2$, $\mu = 0.3$, $P = 125$ kN, and $N_{vb} = 67.50$ kN. When the CFRP plate of the anchorage system reached its ultimate capacity ($F_0 = 78.75$ kN), the assigning load for each bolt N_b was obtained as follows.

$$N_b = \frac{F_0}{2} = 39.38\,\text{kN} < N_{vb} = 67.50\,\text{kN} \tag{14}$$

From the above criterion, the shear-bearing capacity of the bolt satisfied the requirement. When the anchor in this study was used in the strengthened concrete or steel structures, eight bolts sustained the external force at the same time, and the shear-bearing capacity for each bolt met the shear-bearing capacity demand.

After determining the shear-bearing capacity of the bolt, the strength of the weakened steel plate was determined as follows.

$$\sigma = (1 - 0.5n_1/n) \times \frac{N}{A_N} < f \tag{15}$$

The parameter n_1 was the bolt number of the calculated cross section, and n was the bolt number of one side. The parameter N was the external load, and A_N was the net section area of the calculated section, $A_N = (b - n_1 d_0)t$. The parameter d_0 was the diameter of the bolt hole, and b was the width of the steel plate. The parameter t was the thickness of the steel plate, and f was the design strength of the steel plate.

Based on the reference standard of the steel structure, $n_1 = n = 2$, $N = 78.75$ kN, $d_0 = 20$ mm, $b = 120$ mm, $t = 30$ mm, $f = 205$ MPa, and $\sigma = 16.4$ MPa $< f = 205$ MPa, the strength of the weakened steel plate satisfied the standard requirement.

After the load-carrying capacity evaluation of the components for the anchor, the weak component of the anchor was the interface properties of the CFRP/adhesive for the T1 adhesive. Thus, when the interface shear stress exceeded the bond capacity of the CFRP/adhesive, the interface debonding failure was initiated. According to this limiting condition, the maximum anchorage bearing capacity was obtained when the maximum interface shear stress $\sigma_{s1,\text{max-0.4 L}}$ of element 1 was equal to the bond strength $\sigma_{b,\text{T1-60 mm}}$ of the CFRP plate and T1 epoxy.

First, the maximum interface shear force of element 1 was calculated.

$$F_{s1} = A_s \times \sigma_{s1,\text{max}-0.4\,\text{L}} = A_s \times \sigma_{b,T1-60\,\text{mm}} \tag{16}$$

The normal pressure F_p was determined based on Eq. (4).

$$F_{p1} = F_{s1} \times \cot\phi \tag{17}$$

According to the interface bond-friction coefficient μ, the interface friction force F_{f1} was shown as follows.

$$F_{f1} = F_{p1} \times \mu = \mu bl \cot\phi \sigma_{b,T1-60\,\text{mm}} \tag{18}$$

The element external force F_{1*} of element 1 was as follows.

$$F_{1*} = 2 \times F_{f1} = 2\mu bl \cot\phi \sigma_{b,T1-60\,\text{mm}} \tag{19}$$

According to the linear and nonlinear distributions of the interface shear stress and bond-friction coefficient μ, the other element external forces, F_{2*},

$F_{3*}\ldots F_{n*}$, were obtained. Finally, the maximum anchorage bearing capacity $F_{0,\max}$ was determined.

$$F_{0,\max} = F_{1*} + F_{2*} + F_{3*} + \cdots + F_{n*} \quad (20)$$

In this study, the element external force F_{1*} of element 1 was 33.76 kN. Through the linear distribution of the interface shear force, the four element external forces, F_{1*}, F_{2*}, F_{3*} and F_{4*}, of element 1, 2 3, and 4 were 33.76 kN, 26.26 kN, 18.75 kN, and 11.25 kN, respectively. Then, the maximum anchorage bearing capacity $F_{0,\max}$ was predicted to be 90.04 kN. When assuming the CFRP plate was 25 mm × 1.5 mm, the ultimate tensile strength σ_{pc} of the CFRP plate was predicted to be 2401 MPa. The calculation used the T1 adhesive because of its lower interface bond strength. The predicted $F_{0,\max}$ and σ_{pc} were conservative owing the smaller value of the bond-friction coefficient μ based on the friction coefficient between the GFRP plate and steel plate and the larger ratio of the maximum shear stress $\sigma_{s,\max}$ of element 1 with the minimum shear stress $\sigma_{s,\min}$ of element 4, when referring to the experiment results of He et al. Furthermore, the conservative selection of the above two parameters considered a reduction factor of the anchoring CFRP plate in the long-term application and provided a reliable safety factor. Conversely, when the Tc epoxy was chosen as the anchoring adhesive, its in-plane shear strength (22.25 MPa) became the critical parameter. The ultimate anchorage bearing force of the anchor was 105.39 kN, and the maximum tensile strength of the CFRP plate was 2810 MPa.

Based on the above analysis, the interface bond strength of the CFRP/adhesive and the shear strength of the adhesive were two key factors of the ultimate anchorage bearing force. In this study, the Tc adhesive had more potential advantages than the T1 adhesive in anchoring efficiency and ultimate anchorage bearing capacity.

3.2 Validation of the design

To verify the anchoring efficiency of this anchor, tensile tests of the CFRP plate with three anchoring methods were conducted, and the results are listed in Table 2. The failure modes (Al-240-Tc and 240-Tc anchors) are shown in Fig. 8. For convenience, the different anchoring methods of the CFRP plate were referred to as Al-240-Tc, Al-240-T1, and 240-Tc based on the adhesive. Two samples were tested, and the average was applied to evaluate the anchoring efficiency. Meanwhile, two sets of aluminum plates were adopted with the F51 epoxy adhesive at both ends of the CFRP plate to obtain the control tensile strength. From this test, the ultimate tensile load was obtained to be 70.46 kN (± 4.71). The control tensile strength and elongation were 1.95 GPa (± 0.12) and 1.16% (± 0.08), respectively, and the failure mode was a burst of the CFRP plate. The control tensile strength was chosen to be the reference, and the anchorage stress level was recorded as 100% to evaluate the anchoring efficiency of the wedge-extrusion bond anchor.

The first anchoring method (Al-240-Tc) was the wedge-extrusion bond anchor at one end of the CFRP plate and the aluminum plate at the other end. Compared to the control tensile strength, its ultimate tensile load and elongation increased by 9.2% and 6.90%, respectively, and the anchorage stress level reached 109.2%. The minor fluctuation of the data verified that the anchor had a higher load transfer and anchorage bearing capacity than those of the control. The increased ultimate elongation was attributed to the elastic deformation of the Tc epoxy adhesive, which dissipated the energy from the cycling dynamic load, such as the vehicle load, for the anchorage system in long-term use [39]. In addition, the failure mode was the burst of the CFRP plate, and no debonding occurred in the anchor, as shown in Fig. 8.

The second anchoring method (Al-240-Tc) adopted T1 as the filled adhesive. Compared with the Al-240-Tc anchor, the ultimate bearing capacity was similar, and the anchorage stress level was 108.0%. Its ultimate elongation was less than that of the Al-240-Tc anchor, which was relevant to the ultimate deformation of the two adhesives (Table 1). For the Al-240-Tc and Al-240-T1 anchors, their anchorage stress levels exceeded 100%, and the experiment results had agreement with the front mechanical analysis.

The third anchoring method (240-Tc) adopted two sets of 240 anchors, and the adhesive was Tc epoxy. As shown, its ultimate anchoring bearing capacity increased to 80.01 kN, and the anchorage stress level reached 113.6%. The ultimate elongation was 1.25%, nearly consistent with the Al-240-Tc anchor owing to the same adhesive.

Table 2 Verification test results of anchor

Anchoring method	Filled epoxy	Ultimate load (kN)	Anchorage tensile strength (GPa)	Ultimate elongation (%)	Anchorage stress level (%)	Failure mode
Aluminium plate	F51	70.46 (± 4.71)	1.95 (± 0.12)	1.16 (± 0.08)	100	Burst
Aluminium plate/ 240-anchor[a]	F51/Tc	76.94 (± 1.04)	2.07 (± 0.03)	1.24 (± 0.01)	109.2	Burst
Aluminium plate/ 240-anchor[b]	F51/T1	76.34 (± 0.10)	2.05 (± 0.00)	1.17 (± 0.03)	108.0	Burst
240-anchor[c]	Tc	80.01 (± 0.45)	2.15 (± 0.01)	1.25 (± 0.01)	113.6	Burst

[a]One set of aluminum plate and an anchor with a length of 240 mm were used at the both end of CFRP plate, respectively and the filled epoxy in the anchor was Tc. Its name was Al-240-Tc anchor for short

[b]The anchoring method was the same with the second one and the filled adhesive in the anchor was T1. Its name was Al-240-T1 for short

[c]Two sets of anchors with a length of 240 mm were used at the both end of CFRP plate and the filled adhesive in the anchor was Tc. Its name was 240-Tc for short

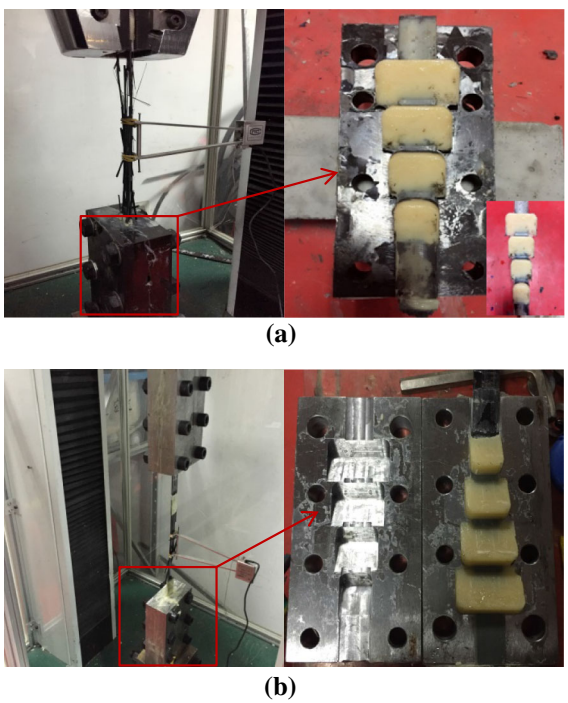

Fig. 8 Tensile failure mode of **a** Al-240-Tc and **b** 240-Tc

Based on the above results, for the universal aluminum plate anchoring method, initial uneven stress or a stress concentration condition at the contact end of the CFRP plate and aluminum plates was formed owing to errors of the sample installation and clamp misalignment. Furthermore, the adverse stress state induced some initial damage (such as a shear crack) on the CFRP plate surface. With the increase of the tensioning force, the initial damage was intensified and extended until the fracture of the CFRP plate owing to inadequate shear resistance capacity. In addition, the adhesive epoxy F51 between the aluminum plate and CFRP plate was too thin to fully absorb the deformation energy, except for the tensile deformation. These factors led to less ultimate tensile strength, ultimate deformation, and greater data fluctuation and dispersion. The obtained tensile strength did not reflect the actual material strength. Conversely, the wedge-extrusion bond anchor adjusted the stress condition of the CFRP plate, avoiding the stress concentration and initial damage of the CFRP plate through the filled ductile and thick epoxy layer in the anchor. Meanwhile, the wedge-extrusion bond anchor reduced the errors of the tensile machine and manual operation to obtain a higher anchoring bearing capacity. The ultimate tensile properties of the CFRP plate were fully developed.

The obtained tensile moduli for the three anchoring methods were approximately equal to the control tensile modulus, which was only dependent on the property of the CFRP plate, in particular the carbon fiber.

Figure 8 shows the tensile failure mode of the anchors, including the Al-240-Tc and 240-Tc anchors. As in the above mechanical analysis, the failure mode of the three anchoring methods was the burst of the CFRP plate, and there was no slippage between the CFRP plate and adhesive in the anchor.

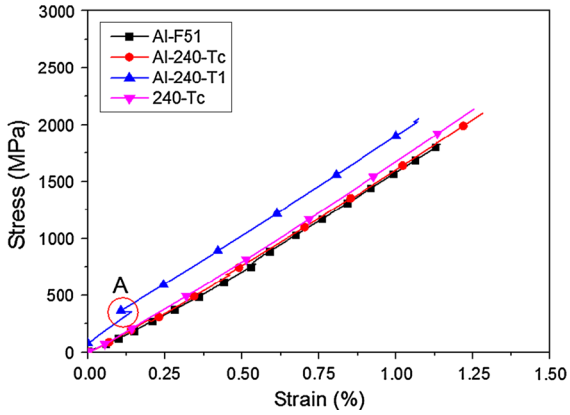

Fig. 9 Relationship of stress and strain of CFRP plates for three anchoring systems

Figure 9 shows the relationship of the stress and strain of the three anchoring systems with the control. The relationship of the stress and strain presented a linear dependence. Furthermore, the slopes of the four curves were approximately the same; therefore, the tensile modulus remained consistent. Inflection point A occurred in the curve of the Al-240-T1 anchoring system because a circular tank epoxy existed outside the anchor during anchoring. When tensioning the anchorage system, the circular tank epoxy separated from the surface of the anchor, and the transient vibration created inflection point A.

4 Conclusions

A wedge-shaped bond anchor was proposed in this study for the rehabilitation of existing structures using prestressed CFRP plates. Two adhesives were designed to compare the anchorage efficiency. The stress distribution in the anchorage zone and maximum anchorage bearing capacity were obtained by numerical and mechanical methods. A tensile test was performed to validate the effectiveness of the proposed anchorage system. The following conclusions were drawn through the mechanical analysis and test results.

With the proposed wedge-extrusion bond anchor, high frictional forces along the CFRP plate were uniformly distributed in the anchorage zone, when the CFRP plate was subjected to tension. The stress concentration that frequently occurs with a traditional mechanical press method would be avoided, and the CFRP plates could be effectively anchored.

From the mechanical analysis, the proposed two adhesives satisfied the anchoring efficiency requirement for this CFRP plate, and the anchors had no debonding failures. The interface bond strength between the CFRP plates and adhesive played a key role in the anchorage system. Based on the critical bond-slip criterion, the ultimate anchorage bearing force of the anchors using the two adhesives was predicted to be 90.04 kN (stiff adhesive) and 105.39 kN (tough adhesive).

The validation test of the anchor showed this wedge-extrusion bond anchor successfully anchored the CFRP plate. A higher anchorage bearing capacity and stress level were obtained, and the ultimate tensile properties of the CFRP plate were fully developed.

Funding This study was funded by the National Key Research and Development Program of China with Grant No. 2017YFC0703007, and the National Natural Science Foundation of China with Grant No. 51478145.

Compliance with ethical standards

Conflict of interest The authors declare that they have no conflict of interest.

References

1. Aslam M, Shafigh P, Jumaat MZ, Shah SNR (2015) Strengthening of RC beams using prestressed fiber reinforced polymers—a review. Constr Build Mater 82: 235–256. https://doi.org/10.1016/j.conbuildmat.2015.02.051
2. Abdulhameed SS, Wu E, Ji B (2015) Mechanical prestressing system for strengthening reinforced concrete members with prestressed carbon-fiber-reinforced polymer sheets. J Perform Constr Facil 29(3):04014081. https://doi.org/10.1061/(ASCE)CF.1943-5509.0000478
3. Michels J, Sena-Cruz J, Czaderski C, Motavalli M (2013) Structural strengthening with prestressed CFRP strips with gradient anchorage. J Compos Constr 17(5):651–661. https://doi.org/10.1061/(ASCE)CC.1943-5614.0000372
4. Wang WW, Dai JG, Harries KA, Zhang L (2014) Prediction of prestress losses in RC beams externally strengthened with prestressed CFRP sheets/plates. J Reinf Plast Compos 33(8):699–713. https://doi.org/10.1177/0731684413519715
5. Xue W, Tan Y, Zeng L (2010) Flexural response predictions of reinforced concrete beams strengthened with prestressed CFRP plates. Compos Struct 92(3):612–622. https://doi.org/10.1016/j.compstruct.2009.09.036

6. Carra G, Carvelli V (2015) Long-term bending performance and service life prediction of pultruded glass fibre reinforced polymer composites. Compos Struct 127:308–315. https://doi.org/10.1016/j.compstruct.2015.03.049
7. Hajihashemi A, Mostofinejad D, Azhari M (2011) Investigation of RC beams strengthened with prestressed NSM CFRP laminates. J Compos Constr 15(6):887–895. https://doi.org/10.1061/(ASCE)CC.1943-5614.0000225
8. Wang Z, Zhao XL, Xian G, Wu G, Singh Raman RK, Al-Saadi S (2017) Long-term durability of basalt- and glass-fibre reinforced polymer (BFRP/GFRP) bars in seawater and sea sand concrete environment. Constr Build Mater 139:467–489. https://doi.org/10.1016/j.conbuildmat.2017.02.038
9. Wang Z, Zhao XL, Xian G, Wu G, Raman RKS, Al-Saadi S (2018) Effect of sustained load and seawater and sea sand concrete environment on durability of basalt- and glass-fibre reinforced polymer (B/GFRP) bars. Corros Sci 138:200–218. https://doi.org/10.1016/j.corsci.2018.04.002
10. Peng H, Zhang J, Cai CS, Liu Y (2014) An experimental study on reinforced concrete beams strengthened with prestressed near surface mounted CFRP strips. Eng Struct 79:222–233. https://doi.org/10.1016/j.engstruct.2014.08.007
11. Motavalli M, Czaderski C, Pfyl-Lang K (2011) Prestressed CFRP for strengthening of reinforced concrete structures: recent developments at Empa, Switzerland. J Compos Constr 15(2):194–205. https://doi.org/10.1061/(ASCE)CC.1943-5614.0000125
12. Ghafoori E, Motavalli M, Nussbaumer A, Herwig A, Prinz GS, Fontana M (2015) Determination of minimum CFRP pre-stress levels for fatigue crack prevention in retrofitted metallic beams. Eng Struct 84:29–41. https://doi.org/10.1016/j.engstruct.2014.11.017
13. Woo SK, Nam JW, Kim JHJ, Han SH, Byun KJ (2008) Suggestion of flexural capacity evaluation and prediction of prestressed CFRP strengthened design. Eng Struct 30(12):3751–3763. https://doi.org/10.1016/j.engstruct.2008.06.013
14. Omran HY, EI-Hacha R (2012) Nonlinear 3D finite element modeling of RC beams strengthened with prestressed NSM-CFRP strips. Constr Build Mater 31:74–85. https://doi.org/10.1016/j.conbuildmat.2011.12.054
15. Ghafoori E, Motavalli M (2015) Normal, high and ultra-high modulus carbon fiber-reinforced polymer laminates for bonded and un-bonded strengthening of steel beams. Mater Design 67:232–243. https://doi.org/10.1016/j.matdes.2014.11.031
16. El-Hacha R, Gaafar M (2011) Flexural strengthening of reinforced concrete beams using prestressed, near-surface-mounted CFRP bars. PCI J 56(4):134–151
17. Ding YH, Ma YJ (2011) Reseach on flexural behavior of reinforced concrete beams strengthened with prestressed near surface mounted CFRP tendons. Adv Mater Res Trans Tech Publ 163:3537–3544. https://doi.org/10.4028/www.scientific.net/AMR.163-167.3537
18. Nordin H, Täljsten B (2006) Concrete beams strengthened with prestressed near surface mounted CFRP. J Compos Constr 10(1):60–68. https://doi.org/10.1061/(ASCE)1090-0268(2006)10:1(60)
19. Triantafillou TC, Deskovic N (1991) Innovative prestressing with FRP sheets: mechanics of short-term behavior. J Eng Mech 117(7):1652–1672. https://doi.org/10.1061/(ASCE)0733-9399(1991)117:7(1652)
20. Huang H, Wang WW, Dai JG, Brigham JC (2017) Fatigue behavior of reinforced concrete beams strengthened with externally bonded prestressed CFRP sheets. J Compos Constr. https://doi.org/10.1061/(ASCE)CC.1943-5614.0000766
21. Hadiseraji M, El-Hacha R (2014) Flexural strengthening of reinforced concrete beams with prestressed externally bonded CFRP sheets. In: 5th international conference on concrete repair-concrete solutions, Belfast, UK, pp 273–277
22. Garden HN, Hollaway LC (1998) An experimental study of the failure modes of reinforced concrete beams strengthened with prestressed carbon composite plates. Compos B Eng 29(4):411–424. https://doi.org/10.1016/S1359-8368(97)00043-7
23. Wang WW, Dai JG, Harries KA, Bao QH (2012) Prestress losses and flexural behavior of reinforced concrete beams strengthened with posttensioned CFRP sheets. J Compos Constr 16(2):207–216. https://doi.org/10.1061/(ASCE)CC.1943-5614.0000255
24. Zoghi M, Foster DC (2006) Post-strengthening prestressed concrete bridges via post-tensioned CFRP-laminates. SAMPE J 42(2):24–30
25. Sayed-Ahmed EY, Lissel SL, Tadros G, Shrive NG (1999) Carbon fibre reinforced polymer (CFRP) post-tensioned masonry diaphragm walls: prestressing, behaviour, and design recommendations. Can J Civil Eng 26(3):324–344. https://doi.org/10.1139/l98-073
26. Ghafoori E, Motavalli M (2015) Innovative CFRP-pre-stressing system for strengthening metallic structures. J Compos Constr 19:04015006. https://doi.org/10.1061/(ASCE)CC.1943-5614.0000559
27. Ghafoori E, Motavalli M, Nussbaumer A, Herwig A, Prinz GS, Fontana M (2015) Design criterion for fatigue strengthening of riveted beams in a 120-year-old railway metallic bridge using pre-stressed CFRP plates. Compos B Eng 68:1–13. https://doi.org/10.1016/j.compositesb.2014.08.026
28. Kianmofrad F, Ghafoori E, Elyasi MM, Motavalli M, Rahimian M (2017) Strengthening of metallic beams with different types of pre-stressed un-bonded retrofit systems. Compos Struct 159:81–95. https://doi.org/10.1016/j.compstruct.2016.09.020
29. Hosseini A, Ghafoori E, Motavalli M, Nussbaumer A, Zhao X-L, Koller R (2018) Prestressed unbonded reinforcement system with multiple CFRP plates for fatigue strengthening of steel members. Polym Basel 10:264. https://doi.org/10.3390/polym10030264
30. Hosseini A, Ghafoori E, Motavalli M, Nussbaumer A, Zhao X-L (2017) Mode I fatigue crack arrest in tensile steel members using prestressed CFRP plates. Compos Struct 178:119–134. https://doi.org/10.1016/j.compstruct.2017.06.056
31. Yang DS, Park SK, Neale KW (2009) Flexural behaviour of reinforced concrete beams strengthened with prestressed carbon composites. Compos Struct 88(4):497–508. https://doi.org/10.1016/j.compstruct.2008.05.016

32. Wu G, Zhao X, Zhou J, Wu Z (2015) Experimental study of RC beams strengthened with prestressed steel-wire BFRP composite plate using a hybrid anchorage system. J Compos Constr 19(2):04014039. https://doi.org/10.1061/(ASCE)CC.1943-5614.0000499
33. Jumaat MZ, Alam MDA (2010) Experimental and numerical analysis of end anchored steel plate and CFRP laminate flexurally strengthened reinforced concrete (r. c.) beams. Int J Phys Sci 5(2):132–144. http://eprints.um.edu.my/id/eprint/6009
34. You YC, Choi KS, Kim JH (2012) An experimental investigation on flexural behavior of RC beams strengthened with prestressed CFRP strips using a durable anchorage system. Compos B Eng 43(8):3026–3036. https://doi.org/10.1016/j.compositesb.2012.05.030
35. Kim YJ, Green MF, Wight RG (2010) Bond and short-term prestress losses of prestressed composites for strengthening PC beams with integrated anchorage. J Reinf Plast Compos 29(9):1277–1294. https://doi.org/10.1177/0731684409102751
36. El-Hacha R, Aly MYE (2013) Anchorage system to prestress FRP laminates for flexural strengthening of steel-concrete composite girders. J Compos Constr 17(3):324–335. https://doi.org/10.1061/(ASCE)CC.1943-5614.0000323
37. Kim YJ, Wight RG, Green MF (2008) Flexural strengthening of RC beams with prestressed CFRP sheets: development of nonmetallic anchor systems. J Compos Constr 12(1):35–43. https://doi.org/10.1061/(ASCE)1090-0268(2008)12:1(35)
38. He J, Xian G (2016) Debonding of CFRP-to-steel joints with CFRP delamination. Compos Struct 153:12–20. https://doi.org/10.1016/j.compstruct.2016.05.100
39. Jiang T, Fang Z (2010) Experimental investigation on the performance of wedge-bond anchors for CFRP tendons. China Civil Eng J 43(2):79–87